JOURNAL OF CATALYSIS 156, 229–242 (1995)

A Kinetic Model of Methanol Synthesis

T. S. Askgaard, J. K. Nørskov, C. V. Ovesen,[1] and P. Stoltze

Center for Atomic-Scale Materials Physics, Physics Department, Building 307, The Technical University of Denmark, DK-2800, Lyngby, Denmark

Received September 12, 1994; revised May 17, 1995; accepted June 12, 1995

A kinetic model of methanol synthesis is presented. All parameters in the model are estimated from gas-phase thermodynamics and surface science studies. The rate-limiting step in the kinetic model was determined from Cu(100) single-crystal experiments to be the hydrogenation of H_2COO* to methoxide and oxide. Calculated methanol rates from the model extrapolated to industrial working conditions were in good agreement with rates measured on a real catalyst. © 1995 Academic Press, Inc.

1. INTRODUCTION

The use of kinetic models based on UHV measurements to analyze the reaction mechanisms of industrial catalysts is very promising (1) and microkinetic models have been derived for a number of catalytic reactions (2–9).

The kinetic model of methanol synthesis presented in this work is an extension of the water–gas shift (WGS) model of Ovesen *et al.* (8, 10).

Methanol synthesis is performed industrially over $Cu/ZnO/Al_2O_3$ catalysts at temperatures of 493–573 K and at pressures 50–100 bar (11, 12). The synthesis gas, manufactured by steam reforming of natural gas (12), usually consists of 5% CO, 5% CO_2, and 90% H_2.

There is still considerable controversy about the chemical state of the catalytically active Cu component and the role of ZnO in $Cu/ZnO/Al_2O_3$ catalysts. It is disputed whether the active phase is copper dissolved in ZnO (13) or metallic copper dispersed on the ZnO surface (14, 15). The activity of $Cu/ZnO/Al_2O_3$ catalysts has been shown to correlate nearly linearly with the area of metallic copper (14, 15), strongly suggesting the metallic copper is the active phase of the catalyst. This is supported by *in situ* X-ray photoelectron spectroscopy (16) and surface X-ray diffraction studies (17).

It was previously accepted that methanol was synthesized from CO and H_2 with CO_2 as a necessary component in the syngas to prevent an irreversible deactivation of the catalyst (13). However, ^{14}C labeling experiments (18, 19) have now confirmed that methanol is mainly produced from the CO_2 component in the feedstock. This is supported by the work of Liu *et al.* (20), and from a recent *in situ* measurement of methanol formation on a working catalyst (21). These results suggest that the methanol synthesis reaction can be described by the following two reactions:

$$CO + H_2O \rightleftharpoons CO_2 + H_2 \quad [1]$$

$$CO_2 + 3H_2 \rightleftharpoons CH_3OH + H_2O. \quad [2]$$

A recent Cu single-crystal experiment by Rasmussen *et al.* (22) has confirmed that copper acts as a catalyst in methanol synthesis using only H_2 and CO_2 in the feed gas. Furthermore, *in situ* infrared vibration spectroscopy measurements by Millar *et al.* (23) have shown that methanol could be synthesized on both a Cu/SiO_2 and a $Cu/ZnO/SiO_2$ catalyst but not on a ZnO/SiO_2 catalyst with a H_2/CO_2 feedstock.

The kinetic model of the methanol synthesis is based on a reaction mechanism deduced from Cu single-crystal experiments. The model will be used to describe and understand the industrial synthesis of methanol over copper-based catalysts. The water–gas shift reaction has been implemented in the kinetic model, since this process takes place on the working catalyst.

A thermodynamic statistical mechanical treatment of the chemisorption process and the competition for free sites between species has been implemented in the model. Incorporation of thermodynamics in the model is necessary to overcome the large pressure and temperature differences between UHV operating conditions and the industrial working conditions of methanol synthesis. In this way, a correct investigation of the methanol reaction mechanism on real catalysts can be performed.

The validity of metallic copper as the active phase will be investigated by comparing predicted methanol rates from the model with measured methanol rates from a real catalyst. For simplicity it is assumed that the dominant

[1] Present address: Haldor Topsøe Research Laboratories, Nymøllevej 55, 2800 Lyngby, Denmark.

0021-9517/95 $12.00

facets of the dispersed Cu particles are the basal planes Cu(100), Cu(110), and Cu(111). Input parameter sets for each of the three low-index planes will be used in the model to analyze the structure sensitivity of the reaction and to propose the active phase in the catalyst.

All input parameters of the model were determined from gas-phase thermodynamics and Cu single crystal experiments. Calculated methanol rates were in agreement with data obtained from a recent Cu single crystal experiment of methanol synthesis at varying temperatures, pressures, and inlet gas compositions (22). The rate-determining step of our proposed reaction mechanism was found to be the hydrogenation of $H_2COO\star$ to methoxide and oxide (22). (A free surface site is symbolized by $\star$ and an adsorbed atom or molecule X is symbolized by $X\star$.) Extrapolation of the model to industrial working conditions of a real catalyst showed a nice correspondence between predicted and measured methanol rates.

The reaction mechanism of the methanol synthesis is presented in Section 2 with a discussion of the experimentally observed reaction paths. Section 3 deals with our proposed kinetic model of the methanol synthesis, where the net rates of water and methanol synthesis are derived in detail. A description of the selected input parameters will be given in Section 4. A test of the model and investigations of the coverages of the species, reaction orders, and the overall activation enthalpy, will be performed in Section 5. Final remarks regarding the results of this work are given in Section 6.

TABLE 1

Elementary Steps in the Kinetic Model of Methanol Synthesis

Steps	Surface reactions
1	$H_2O(g) + \star \rightleftharpoons H_2O\star$
2	$H_2O\star + \star \rightleftharpoons OH\star + H\star$
3	$2OH\star \rightleftharpoons H_2O\star + O\star$
4	$OH\star + \star \rightleftharpoons O\star + H\star$
5	$2H\star \rightleftharpoons H_2 + 2\star$
6	$CO(g) + \star \rightleftharpoons CO\star$
7	$CO\star + O\star \rightleftharpoons CO_2\star + \star$
8	$CO_2\star \rightleftharpoons CO_2(g) + \star$
9	$CO_2\star + H\star \rightleftharpoons HCOO\star + \star$
10	$HCOO\star + H\star \rightleftharpoons H_2COO\star + \star$
11	$H_2COO\star + H\star \rightleftharpoons H_3CO\star + O\star$
12	$H_3CO\star + H\star \rightleftharpoons CH_3OH\star + \star$
13	$CH_3OH\star \rightleftharpoons CH_3OH(g) + \star$
14	$H_2COO\star + \star \rightleftharpoons HCHO\star + O\star$
15	$HCHO\star \rightleftharpoons HCHO(g) + \star$
16	$H_2COO\star + H\star \rightleftharpoons HCHO\star + OH\star$

Note. A free surface site is symbolized by $\star$ and an adsorbed atom or molecule X is symbolized by $X\star$.

2. REACTION MECHANISM

Nakamura *et al.* (24–26) have analyzed two different reaction mechanisms for the water–gas shift reaction. In the *surface-redox* mechanism, $H_2O(g)$ is completely dissociated to $O\star$ and $H_2(g)$, and the surface oxide $O\star$ is removed by $CO\star$ to produce $CO_2(g)$. In the *formate* mechanism, $H_2O\star$ dissociates to $OH\star$ and $H\star$, and formate $HCOO\star$ is synthesized by the reaction of $CO\star$ with $OH\star$. $H_2(g)$ and $CO_2(g)$ are then eventually produced by the thermal decomposition of formate. Strong evidence for the surface-*redox* mechanism was found from Cu single-crystal studies (24–26).

The first eight elementary steps in Table 1 is the redox mechanism of the WGS reaction proposed by Nakamura *et al.* (24), and the formulated kinetic model has been analyzed in great detail by Ovesen *et al.* (8).

Infrared vibration spectroscopy and temperature-programmed reaction studies have confirmed the existence of the formate species $HCOO\star$ (27, 28). Synthesis of formate has been performed on a Cu(100) single crystal exposed to a CO_2:H_2 gas mixture, and the formate species was identified with X-ray photoelectron spectroscopy, electron energy-loss spectroscopy, and temperature-programmed desorption (29).

There is spectroscopic evidence for the existence of $H_2COO\star$ on Ag(110) (30, 31), and the presence of $H_2COO\star$ on Cu(110) has been verified from interpretations of temperature-programmed reaction data (32).

Methanol and formaldehyde are molecularly adsorbed on Cu(110), as shown by electron energy-loss spectroscopy and temperature-programmed desorption (33–35). The direct oxidation of formaldehyde to $H_2COO\star$ has been observed with temperature-programmed reaction spectroscopy (32).

A temperature-programmed reaction spectroscopy study of a preoxidized Cu(110) surface exposed to methanol (35) verified the dissociative adsorption of methanol to $H\star$ and methoxide $H_3CO\star$, oxidation of methoxide to $H\star$ and $H_2COO\star$, decomposition of $H_2COO\star$ to $H\star$ and $HCOO\star$, and finally, decomposition of formate to CO_2 and H_2 at $T = 470$ K. Hydrogenation of methoxide to methanol has been confirmed (35), but an experimental verification of formate hydrogenation to methoxide has not been reported yet. An investigation of formate hydrogenation on Cu(100) has been performed, but it was not possible to identify the products, because the yields were too low to be detected (29, 36).

The elementary steps 9–13 in Table 1 constitute the simplest reaction mechanism of the methanol synthesis reaction. The kinetic model of methanol synthesis will be based on all the elementary steps 1–13 in Table 1. Steps

14–16 describe possible pathways leading to formaldehyde as a by-product.

3. KINETIC MODEL

Kinetic models have been formulated with either step 10, 11, or 12 as the rate-determining step in the reaction mechanism (Table 1). Each model was analyzed using data from a recent Cu single-crystal experiment by Rasmussen *et al.* (22), and the rate-determining step in the methanol synthesis reaction was deduced to be the hydrogenation of $H_2COO\star$ to methoxide and oxide.

We will here give a description of the procedure used to formulate the kinetic model with step 11 as the rate-determining step. The models with step 10 and step 12 as the rate-determining step have been derived in an analogous way.

Our kinetic model is an extension of the WGS model (8), with the following set of rate and equilibrium equations:

$$K_1 \frac{p_{H_2O}}{p_o}\theta_\star = \theta_{H_2O\star} \quad [3]$$

$$r_2 = k_2\theta_{H_2O\star}\theta_\star - \frac{k_2}{K_2}\theta_{OH\star}\theta_{H\star} \quad [4]$$

$$K_3\theta_{OH\star}^2 = \theta_{H_2O\star}\theta_{O\star} \quad [5]$$

$$r_4 = k_4\theta_{OH\star}\theta_\star - \frac{k_4}{K_4}\theta_{O\star}\theta_{H\star} \quad [6]$$

$$K_5\theta_{H\star}^2 = \frac{p_{H_2}}{p_o}\theta_\star^2 \quad [7]$$

$$K_6\frac{p_{CO}}{p_0}\theta_\star = \theta_{CO\star} \quad [8]$$

$$r_7 = k_7\theta_{CO\star}\theta_{O\star} - \frac{k_7}{K_7}\theta_{CO_2\star}\theta_\star \quad [9]$$

$$K_8\theta_{CO_2\star} = \frac{p_{CO_2}}{p_o}\theta_\star \quad [10]$$

$$K_9\theta_{H\star}\theta_{CO_2\star} = \theta_{HCOO\star}\theta_\star \quad [11]$$

$$K_{10}\theta_{HCOO\star}\theta_{H\star} = \theta_{H_2COO\star}\theta_\star \quad [12]$$

$$r_{11} = k_{-11}K_{11}\theta_{H_2COO\star}\theta_{H\star} - k_{-11}\theta_{H_3CO\star}\theta_{O\star} \quad [13]$$

$$K_{12}\theta_{H_3CO\star}\theta_{H\star} = \theta_{CH_3OH\star}\theta_\star \quad [14]$$

$$K_{13}\theta_{CH_3OH\star} = \frac{p_{CH_3OH}}{p_o}\theta_\star. \quad [15]$$

K_i are the equilibrium constants calculated from the molecular partition functions of the intermediates, k_i are the rate constants assumed to be of the Arrhenius form, $\theta_{X\star}$ is the coverage of the species $X\star$, and p_o is the thermodynamic reference pressure. In the present model, one active site is defined as two Cu sites, and $\theta_\star = 1$ corresponds to a $c(2 \times 2)$ surface structure.

The coverages of O$\star$ and OH$\star$ must be stationary at each point in the bed of a catalyst operating in steady state. A mass balance study of O$\star$ and OH$\star$ (Table 1) gives us then the following relationship between the slow reaction steps (8):

$$r_7 - r_{11} = \frac{1}{2}(r_2 + r_4). \quad [16]$$

In explicit form a second-order equation is obtained,

$$a\frac{\theta_{O\star}}{\sigma_\star} + b\left(\frac{\theta_{O\star}}{\theta_\star}\right)^{1/2} + c = 0, \quad [17]$$

where the following short-hand notations have been used:

$$\begin{aligned} a &= 2k_7K_6\frac{p_{CO}}{p_o} + 2k_{-11}\frac{1}{K_{12}K_{13}}\frac{p_{CH_3OH}}{p_o}\left(\frac{p_{H_2}}{K_5p_o}\right)^{-1/2} \\ &\quad + \frac{k_4}{K_4}\left(\frac{p_{H_2}}{K_5p_o}\right)^{1/2} \\ b &= \frac{k_2}{K_2}\left(\frac{K_1}{K_3K_5}\frac{p_{H_2}p_{H_2O}}{p_o}\frac{p_{H_2O}}{p_o}\right)^{1/2} - k_4\left(\frac{K_1}{K_3}\frac{p_{H_2O}}{p_o}\right)^{1/2} \\ c &= -2\frac{k_7}{K_7K_8}\frac{p_{CO_2}}{p_o} - k_2K_1\frac{p_{H_2O}}{p_o} \\ &\quad - 2k_{-11}K_{11}\frac{K_9K_{10}}{K_8}\frac{p_{CO_2}}{p_o}\left(\frac{p_{H_2}}{K_5p_o}\right)^{3/2}. \end{aligned} \quad [18]$$

It is now possible to relate all the coverages of the intermediates to $\theta_\star$,

$$\theta_{O\star} = \left(\frac{-b + \sqrt{b^2 - 4ac}}{2a}\right)^2\theta_\star \quad [19]$$

$$\begin{aligned} \theta_{OH\star} &= \left(\frac{K_1}{K_3}\frac{p_{H_2O}}{p_o}\theta_{O\star}\theta_\star\right)^{1/2} \\ &= \left(\frac{K_1}{K_3}\frac{p_{H_2O}}{p_o}\right)\left(\frac{-b + \sqrt{b^2 - 4ac}}{2a}\right)\theta_\star \end{aligned} \quad [20]$$

$$\theta_{H\star} = \sqrt{\frac{p_{H_2}}{K_5p_o}}\theta_\star \quad [21]$$

$$\theta_{H_2O*} = K_1 \frac{p_{H_2O}}{p_o} \theta_* \quad [22]$$

$$\theta_{CO*} = K_6 \frac{p_{CO}}{p_o} \theta_* \quad [23]$$

$$\theta_{CO_2*} = \frac{1}{K_8} \frac{p_{CO_2}}{p_o} \theta_* \quad [24]$$

$$\theta_{HCOO*} = \frac{K_9}{K_8} \sqrt{\frac{p_{H_2}}{K_5 p_o}} \frac{p_{CO_2}}{p_o} \theta_* \quad [25]$$

$$\theta_{H_2COO*} = \frac{K_9 K_{10}}{K_5 K_8} \frac{p_{H_2}}{p_o} \frac{p_{CO_2}}{p_o} \theta_* \quad [26]$$

$$\theta_{H_3CO*} = \frac{1}{K_{12} K_{13}} \frac{p_{CH_3OH}}{p_o} \left(\frac{p_{H_2}}{K_5 p_o} \right)^{-1/2} \theta_* \quad [27]$$

$$\theta_{CH_3OH*} = \frac{1}{K_{13}} \frac{p_{CH_3OH}}{p_o} \theta_*. \quad [28]$$

From the conservation law $\Sigma_i \theta_i = 1$, the coverage of free sites is extracted to be

$$\begin{aligned} \theta_*^{-1} = 1 &+ \sqrt{\frac{p_{H_2}}{K_5 p_o}} + K_1 \frac{p_{H_2O}}{p_o} + K_6 \frac{p_{CO}}{p_o} \\ &+ \frac{1}{K_8} \frac{p_{CO_2}}{p_o} + \sqrt{\frac{K_1 p_{H_2O}}{K_3 p_o}} \left(\frac{-b + \sqrt{b^2 - 4ac}}{2a} \right) \\ &+ \frac{K_9}{K_8} \sqrt{\frac{p_{H_2}}{K_5 p_o}} \frac{p_{CO_2}}{p_o} + \frac{K_9 K_{10}}{K_5 K_8} \frac{p_{H_2}}{p_o} \frac{p_{CO_2}}{p_o} \\ &+ \frac{1}{K_{13}} \frac{p_{CH_3OH}}{p_o} + \frac{1}{K_{12} K_{13}} \frac{p_{CH_3OH}}{p_o} \left(\frac{1}{K_5} \frac{p_{H_2}}{p_o} \right)^{-1} \\ &+ \left(\frac{-b + \sqrt{b^2 - 4ac}}{2a} \right)^2. \end{aligned} \quad [29]$$

In this way an explicit solution for all the coverages was obtained. The net rate of the water and the methanol synthesis is then given by the equations

$$r_{CH_3OH} = k_{-11} K_{11} K_{10} \frac{\theta_{HCOO*} \theta_{H*}^2}{\theta_*} - k_{-11} \theta_{H_3CO*} \theta_{O*}$$

$$r_{H_2O} = k_{-11} K_{11} K_{10} \frac{\theta_{HCOO*} \theta_{H*}^2}{\theta_*} - k_{-11} \theta_{H_3CO*} \theta_{O*}$$

$$- k_7 \theta_{CO*} \theta_{O*} + \frac{k_7}{K_7} \theta_{CO_2*} \theta_*,$$

with $k_{11} = k_{-11} K_{11}$. The reverse rate constant of reaction step 11 is symbolized by k_{-11}. The rate constant k_{-11} was deduced from methanol synthesis experiments on Cu(100) (22). The advantage of selecting k_{-11} as a fitting parameter, instead of k_{11}, is that the partition function z_{H_2COO*} cancels out in the product term $K_{10} K_{11}$. A reliable estimate of the fitting parameter can then be obtained if the coverage of H_2COO* is small.

The net rate of all reaction steps in Table 1 must be zero at gas-phase equilibrium. As a consequence, the coverage of all species are explicitly defined by the external gas composition and the equilibrium constants calculated from molecular partition functions. Requiring all rates to be zero, it is straightforward to show that the equilibrium constant K_G of the gas phase reaction

$$CO_2 + 3H_2 \rightleftharpoons CH_3OH + H_2O \quad [30]$$

is related to the model equilibrium constants in the following way:

$$\begin{aligned} K_G &= \frac{p_{CH_3OH} p_{H_2O} p_o^2}{p_{H_2}^3 p_{CO_2}} \\ &= K_1^{-1} K_2^{-1} K_4^{-1} K_5^{-3} K_8^{-1} K_9 K_{10} K_{11} K_{12} K_{13}. \end{aligned} \quad [31]$$

Inserting K_G in the net rate expression gives the result

$$\begin{aligned} r_{CH_3OH} = k_{-11} K_5^{-3/2} K_8^{-1} K_9 K_{10} K_{11} \\ \left\{ \left(\frac{p_{H_2}}{p_o} \right)^{3/2} \left(\frac{p_{CO_2}}{p_o} \right) - x \right\} \theta_*^2 \end{aligned} \quad [32]$$

with the shorthand notation

$$x = \frac{1}{K_G K_2 K_4} \left(\frac{\theta_{O*} \theta_{H*}^2}{\theta_{H_2O*} \theta_*^2} \right) \frac{p_{CH_3OH} p_{H_2O}}{p_{H_2}^{3/2} p_o^{1/2}}. \quad [33]$$

The net rate, r, is uniquely split into the difference between r_+ and r_-, if step 2 makes several turnovers in both directions compared to step 7,

$$r = r_+ - r_- \quad [34]$$

$$r_+ = k_{-11} K_5^{-3/2} K_8^{-1} K_9 K_{10} K_{11} \left(\frac{p_{H_2}}{p_o} \right)^{3/2} \left(\frac{p_{CO_2}}{p_o} \right) \theta_*^2 \quad [35]$$

$$r_- = k_{-11} K_5^{-3/2} K_8^{-1} K_9 K_{10} K_{11} \frac{1}{K_G} \frac{p_{CH_3OH} p_{H_2O}}{p_{H_2}^{3/2} p_o^{1/2}} \theta_*^2. \quad [36]$$

Introducing K_G clearly demonstrates that the net rate r is equal to zero at thermodynamic equilibrium.

TABLE 2

Rate Constants for Cu(111) Used in the Kinetic Model

$A_2 = 2.6 \times 10^{14}$ s^{-1}	$E_2 = 114.0$ kJ mol^{-1}
$A_4 = 2.3 \times 10^{8}$ s^{-1}	$E_4 = 99.1$ kJ mol^{-1}
$A_7 = 1.1 \times 10^{13}$ s^{-1}	$E_7 = 72.2$ kJ mol^{-1}
$A_9 = 2.1 \times 10^{10}$ s^{-1}	$E_9 = 78.0$ kJ mol^{-1}
$A_{11} = 7.8 \times 10^{20}$ s^{-1}	$E_{11} = 161.8$ kJ mol^{-1}

4. MODEL PARAMETERS

General techniques used to determine the model parameters of the WGS mechanism have been published previously (8), and we have obtained essentially the same results. The extra input parameters of our methanol model are listed in Tables 2 and 3.

TABLE 3

Table of Thermodynamic Data for Cu(111) Used in the Kinetic Model of the Methanol Synthesis

Species	Parameters
HCOO*	$\nu_\perp = 322.0$ cm^{-1}, $\nu_\parallel = 35.51(2)$ cm^{-1}, $\nu_r = 400.0(3)$ cm^{-1}, $\nu_1 = 758$ cm^{-1}, $\nu_2 = 1331$ cm^{-1}, $\nu_3 = 1640$ cm^{-1}, $\nu_4 = 2879$ cm^{-1}, $\nu_5 = 1073$ cm^{-1}, $\nu_6 = 1377$ cm^{-1}, and $E_g = -552.7$ kJ mol^{-1}
CH_3O*	$\nu_\perp = 400.00$ cm^{-1}, $\nu_\parallel = 36.49(2)$ cm^{-1}, $\nu_r = 360.0(3)$ cm^{-1}, $\nu_1 = 1020.0$ cm^{-1}, $\nu_2 = 1150.0(2)$ cm^{-1}, $\nu_3 = 1460.0(3)$ cm^{-1}, $\nu_4 = 2840.0$ cm^{-1}, $\nu_5 = 2940.0(2)$ cm^{-1}, and $E_g = -300.0$ kJ mol^{-1}
H_2COO*	$\nu_\perp = 405.00$ cm^{-1}, $\nu_\parallel = 29.95(2)$ cm^{-1}, $\nu_r = 400.0(3)$ cm^{-1}, $\nu_1 = 630.0$ cm^{-1}, $\nu_2 = 960.0$ cm^{-1}, $\nu_3 = 1090.0$ cm^{-1}, $\nu_4 = 1220.0(2)$ cm^{-1}, $\nu_5 = 1420.0$ cm^{-1}, $\nu_6 = 1480.0$ cm^{-1}, $\nu_7 = 2920.0$ cm^{-1}, $\nu_8 = 3000.0$ cm^{-1}, and $E_g = -568.0$ kJ mol^{-1}
CH_3OH	$I_A = 6.578 \times 10^{-47}$ kg m^2, $I_B = 34.004 \times 10^{-47}$ kg m^2, $I_C = 35.306 \times 10^{-47}$ kg m^2, $\sigma = 3$, $\nu_1 = 270$ cm^{-1}, $\nu_2 = 1033$ cm^{-1}, $\nu_3 = 1060$ cm^{-1}, $\nu_4 = 1165$ cm^{-1}, $\nu_5 = 1345$ cm^{-1}, $\nu_6 = 1477(2)$ cm^{-1}, $\nu_7 = 1455$ cm^{-1}, $\nu_8 = 2844$ cm^{-1}, $\nu_9 = 2960$ cm^{-1}, $\nu_{10} = 3000$ cm^{-1}, $\nu_{11} = 3681$ cm^{-1}, and $E_g = -342.8$ kJ mol^{-1}
CH_3OH*	$\nu_\perp = 290.0$ cm^{-1}, $\nu_\parallel = 35.51(2)$ cm^{-1}, $\nu_r = 360.0(3)$ cm^{-1}, $\nu_1 = 750$ cm^{-1}, $\nu_2 = 820$ cm^{-1}, $\nu_3 = 1030$ cm^{-1}, $\nu_4 = 1150(2)$ cm^{-1}, $\nu_5 = 1470(3)$ cm^{-1}, $\nu_6 = 2860$ cm^{-1}, $\nu_7 = 2970(2)$ cm^{-1}, $\nu_8 = 3320$ cm^{-1}, and $E_g = -413.3$ kJ mol^{-1}

Note. B, I_B, and σ are the rotational constant, the moment of inertia, and the symmetry number of the gas-phase molecule, respectively. Vibrational modes are denoted by ν_j with $j = 1 - j_{max}$, and the degeneracy of a frequency is enclosed in parentheses. The frequencies $\nu_\perp$, $\nu_\parallel$, and ν_r are the frustrated translational orthogonal frequency, the frustrated translational parallel frequency, and the frustrated rotational frequency, respectively (4).

Temperature-programmed desorption results of formate decomposition on Cu(100) (29) were analyzed to deduce the ground state energy E_g of chemisorbed formate. We defined the rate constant of formate decomposition as $k_{-9} = k_9 K_9$. The equilibrium constant K_9 is a function of E_g, and the extraction of the ground state energy was performed by a best fit to the temperature-programmed desorption curves.

Published results of formate synthesis on Cu(100) (29) were used to determine the rate constant of formate synthesis k_9. A kinetic model was presented in Ref. (29) which consisted of three steps equivalent to steps 5, 8, and 9 in our model,

$$\theta_{H*} = \sqrt{\frac{p_{H_2}}{K_5 p_0}}\,\theta_*$$

$$\theta_{CO_2*} = \frac{1}{K_8}\frac{p_{CO_2}}{p_0}\,\theta_*$$

$$\theta_* = 1 - \theta_{HCOO*} \Big/ 1 + \left(\frac{1}{K_5}\frac{p_{H_2}}{p_0}\right)^{1/2} + \frac{1}{K_8}\frac{p_{CO_2}}{p_0} \qquad [37]$$

$$\frac{d\theta_{HCOO*}}{dt} = k_9 \theta_{CO_2*} \theta_{H*} - \frac{k_9}{K_9}\,\theta_{HCOO*}\theta_*.$$

In the investigation of the model by the authors of Ref. (29) a repulsive formate–formate interaction energy of 14 kJ mol^{-1} was introduced to explain the measured data. We have analyzed the published data using the same kinetic model with no pairwise interactions of species except for the usual interaction limiting the saturation coverage to one molecule per site. Measured data were reproduced successfully without the formate–formate repulsion if $\theta_{HCOO*} \leq 0.20$ ml. The competition for free surface sites at a higher coverage of formate requires a more detailed statistical mechanical treatment. For simplicity we neglect the formate–formate interaction and only use points with $\theta_{HCOO*} \leq 0.20$ ml in the calculation of the rate constant k_9. Calculations of the coverages under reaction conditions, Section 5.4, show that the coverage of formate is indeed low at typical methanol synthesis conditions. The activation energy in the reverse direction (step 9) was calculated to be $E^{\ddagger}_{-9} = 120.0$ kJ mol^{-1}, very close to the measured activation energy $E^{\ddagger} = 129.0$ kJ mol^{-1} of formate decomposition on Cu(110) (35, 37). The value of E_g was required in the evaluation of k_9, but this problem was solved by repeating the fitting procedures of E_g and k_9 until a self-consistent solution was obtained.

Methoxide decomposes to formaldehyde and hydrogen at approximately 365 K on Cu(110) (35). It is less stable than the formate species, which decomposes to hydrogen and carbon dioxide at approximately 470 K. A large steady-state concentration of copper formate has been observed

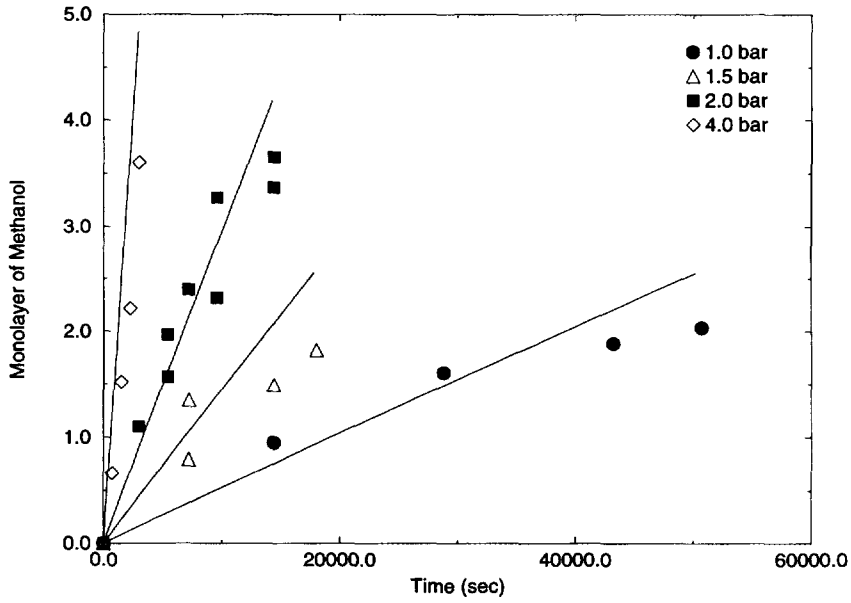

FIG. 1. Total pressure variation with gas composition $H_2:CO_2 = 1:1$ and temperature $T = 543$ K on Cu(100).

on a working methanol synthesis catalyst at industrial operating conditions (23). The methoxide species was not detected, which indicates that the surface concentration of methoxide must be very small during the methanol synthesis. Experimental data are not available for a calculation of the ground-state energy of methoxide, and to ensure a low coverage of methoxide the following value has therefore been chosen: $E_g = -300.0$ kJ mol^{-1}.

The stability of $H_2COO\star$ cannot be directly calculated because the decomposition of $H_2COO\star$ to hydrogen and formate occurs at $T \approx 260$ K on Cu(110) below the hydrogen desorption temperature at $T \approx 340$ K (31, 32). To ensure a low coverage of the species the ground state energy has been estimated to be $E_g = -568.0$ kJ mol^{-1}.

The rate constant k_{11} was deduced from Cu single-crystal measurements (22) of methanol formation to be discussed in the next section.

5. DISCUSSION

5.1. Turnover Rates on Cu(100)

Three kinetic models were formulated with step 10, 11, or 12 as the rate determining step in our proposed reaction mechanism (Table 1). The rate constant k_m (m = 10, 11, or 12) was extracted from published results of methanol formation on a Cu(100) surface exposed to a feed of $H_2:CO_2 = 1:1$ at 2 bar and varying temperatures in the range $T = 483$–563 K (22).

Each kinetic model was tested against independent sets of methanol data obtained from the Cu(100) crystal experiment (22) with varying pressures and changes in the synthesis gas composition. The hydrogenation of $H_2COO\star$ to methoxide and oxide was found to be the correct rate-limiting step. Arrhenius parameters of the rate constant k_{11} are given in Table 2.

The model was first tested against methanol formation data obtained with a feed gas of $H_2:CO_2 = 1:1$ at constant temperature $T = 543$ K and varying pressures (22). the predicted formation of methanol as a function of exposure time correlates well with the measured data (Fig. 1). A second test of the model was the comparison of predicted rates and rates measured on the Cu(100) crystal exposed to different synthesis gas compositions at constant temperature $T = 543$ K and constant pressure $p = 2$ bar (Fig. 2). The agreement is acceptable taking into account an estimated uncertainty of 20% of the measured data (22). The agreement suggests that the rate-limiting step of methanol synthesis is indeed one of the steps, 10, 11, or 12, with step 11 begin the most likely candidate.

5.2. Turnover Rates on Real Catalysts

An investigation of the implemented WGS mechanism in the model has been performed using low-pressure WGS results published by Herwijnen *et al.* (38, 39). Initial WGS rates as a function of the mole fraction of water were measured using a plug flow reactor designed to give conversions below 12% of equilibrium (Fig. 3). The experiments were performed with a Cu/ZnO catalyst in the temperature range $T = 445$–501 K, total pressure $p = 1$ atm, and varying feed gas mixtures of CO, H_2O, and nitrogen.

We have used input parameter sets from Cu(100), Cu(111), and Cu(110) to analyze the structure sensitivity

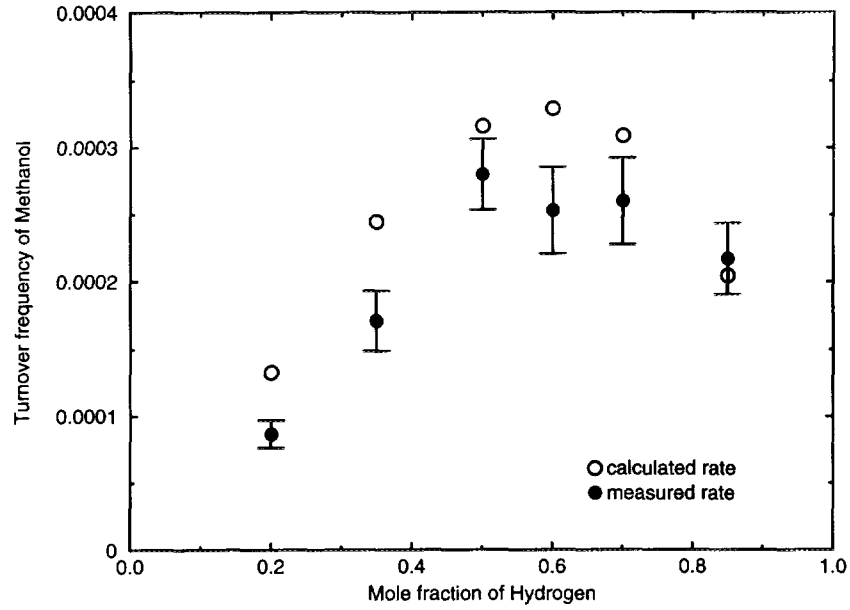

FIG. 2. Change of $H_2:CO_2$ gas composition at constant T = 543 K and p = 2 bar on Cu(100). Solid circles represent measured rates and open circles represent model predictions.

of the catalyst. It was only possible to obtain a good reproduction of the experimental data with the Cu(111) parameter set. This result indicates that copper is the catalytically active component in the catalyst with a dominant Cu(111) facet. The larger area of the Cu(111) facet among the three facets studied can be given a natural explanation from the Wulff construction, because of the lower surface energy determined by the more close-packed surface structure. This observation is in agreement with computer simulations of Cu clusters at high temperatures, where the dominant surface facets could be identified with close-packed surface structures after annealing (40).

Graaf *et al.* (41, 42) have measured the activity of a commercial $Cu/ZnO/Al_2O_3$ catalyst at pressures p = 15–50 bar, temperatures T = 483–518 K, and by varying flow rates and gas mixtures of $H_2:CO_2:CO$. A spinning basket

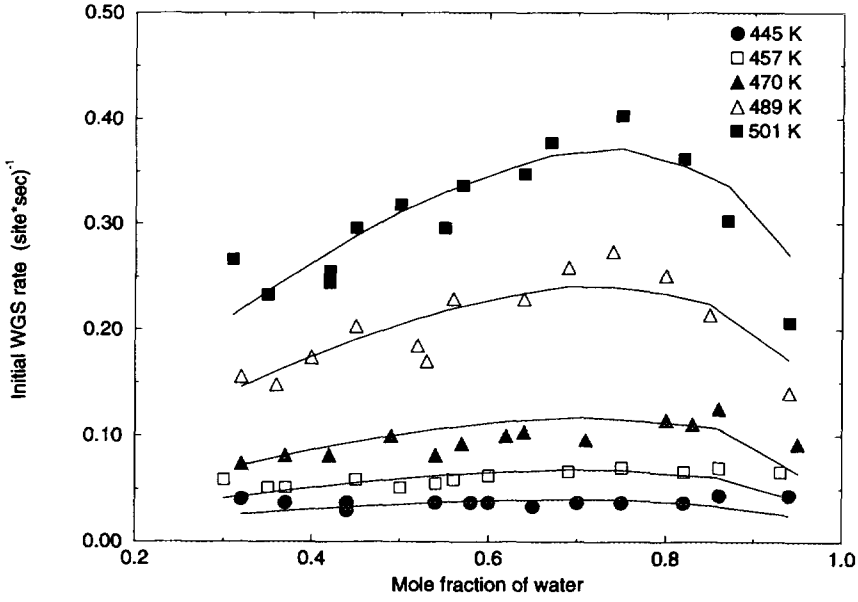

FIG. 3. Initial WGS rates as a function of the mole fraction of water. The solid lines are the model predictions of the initial rates.

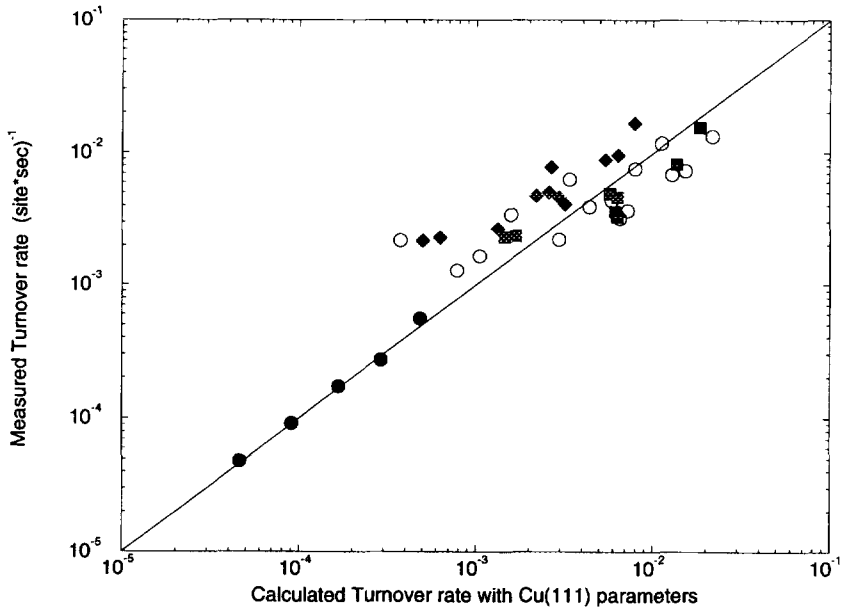

FIG. 4. Measured versus calculated turnover frequency of methanol. Total pressures are 15, 30, and 50 bar. Temperatures are 483.5, 499.3, and 516.7 K. Diamonds, inlet gas composition $H_2:CO:CO_2 = 85.9:12.0:2.1$; squares, inlet gas composition $H_2:CO:CO_2 = 75.4:17.9:6.7$; and circles, inlet gas composition $H_2:CO:CO_2 = 90.0:5.3:4.7$.

reactor was used which kept the catalyst particles in four baskets on a stirrer shaft. With this setup high mass and heat transfer rates were obtained between the gas and catalyst, insuring that the catalyst bed was exposed to the same gas composition. The mole fractions of the components in the exit gas composition were measured with a GLC apparatus, except for hydrogen, which was determined from a total material balance. The reaction rates for water and methanol were calculated from mixed-flow material balances over the reactor (41, 42).

The Cu area of the catalyst is taken from (21), and a direct comparison of the measured rates with model predictions can be performed (Fig. 4). Our kinetic model was extrapolated to the working conditions of Graaf's experiments (41, 42), and an agreement between measured and model-predicted turnover rates is expected if the active phase of the catalyst is metallic copper. Before beginning our analysis, we performed a critical study of the published data from Graaf *et al.* (41, 42). Since they observed intraparticle diffusion limitations at temperatures above 518 K, these data points were ignored in our comparison. Also, their measured exit mole fraction of methanol was compared to a theoretical mole fraction determined from material balances of hydrogen, carbon, and oxygen. A comparison of the expected and measured mole fraction of methanol demonstrated that not all published data points could have been obtained from the catalyst operating in steady state, since relative errors up to 100% were found. All the data points from the three inlet gas compositions shown in Fig. 4 have relative errors below 40%.

Figure 4 illustrates the agreement between measured and model-predicted turnover rates. The good agreement between calculated and measured rates demonstrates that it is possible to use Cu single-crystal data to predict the rate of methanol synthesis over an industrial catalyst. However, a trend between the data points from three different inlet gas compositions can be observed. The measured methanol rates with a high p_{CO}/p_{CO_2} ratio are greater than the predicted rates, and the measured methanol rates with a small p_{CO}/p_{CO_2} ratio are below the predicted rates. These observations suggest that step 12 in Table 1 could be the rate-determining step. The forward net rate would then be proportional to the correlation factor p_{CO}/p_{CO_2}, if step 7 makes several turnovers for each turnover of the net reaction. To test this hypothesis, a new model with step 12 as the rate-limiting step was constructed and tested against the catalyst data. However, the predicted rates were found to be unacceptably high (43) compared with the measured data, and a kinetic model with step 12 as rate determining is not very likely. This conclusion is supported by the Cu(100) single-crystal experiments discussed in Section 5.1, where the rate-determining step was found to be step 11.

Another interesting explanation of the systematic deviation of the data points in Fig. 4 was given by Clausen *et al.* (44). It was suggested that the total copper area of a working catalyst depends on the oxidation potential of the synthesis gas. Calculations of the morphology change of supported copper particles with the Wulff construction verified that the copper area can change significantly if the

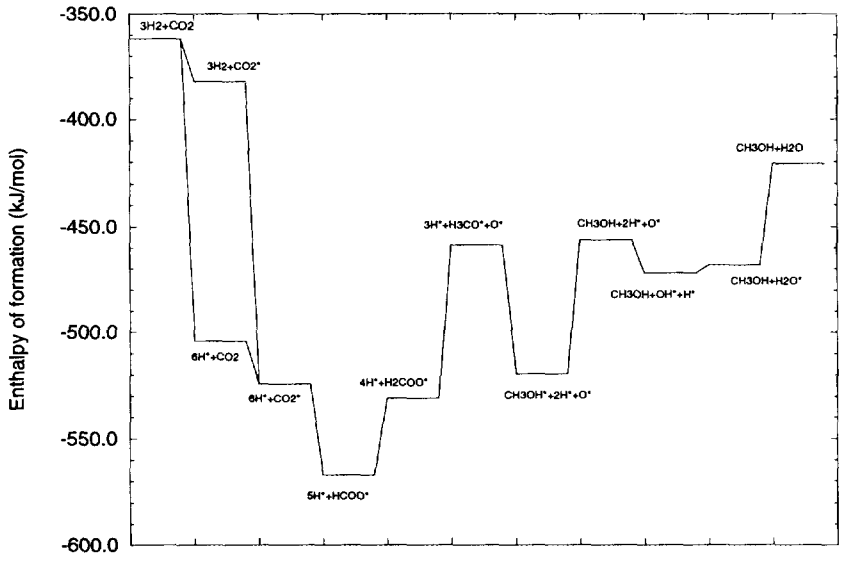

FIG. 5. Enthalpy of formation on Cu(111) at T = 543 K, p = 2 atm, and θ = 0.5 for the methanol synthesis.

interface energy between copper and support is changed (44). This effect has direct consequences for the methanol synthesis catalyst, which is composed of metallic Cu particles dispersed on ZnO. A relatively large CO content in the gas composition will have a reducing influence on the ZnO, and the removal of oxygen in the interface region between copper and ZnO will have an impact on the surface shape of the Cu crystallites (44). The shape of the copper particles on zinc will become thinner, since the interface energy of Cu–Zn is lower than the interface energy of Cu–ZnO. The total surface area of copper in the catalyst will thus be increased with a high reduction potential of the synthesis gas. Implementing a correction factor proportional to the ratio p_{CO}/p_{CO_2} in the rate equation of methanol production could possibly eliminate the systematic deviations observed in Fig. 4.

Overall, reasonably good agreement between measured and predicted rates is observed, considering the uncertainty of the measured methanol rate and the possibility of *in situ* morphology changes of the metallic Cu particles in a working catalyst. In no case is the calculated rate off by more than a factor of two, except for a few data points at conditions where the measured turnover rate is below 1×10^{-3} site $\times$ s^{-1}. This is as good as can be expected from the present model, which is based on a mean field description of adsorbates with no adsorbate–adsorbate interactions except the usual nearest neighbor repulsion limiting the saturation to one molecule per site.

5.3. Thermodynamic Stability

The methanol process, $3H_2 + CO_2 \rightleftharpoons CH_3OH + H_2O$, is exothermic with a negative reaction volume and thus favored by low temperatures and high pressures. However, a selfinhibition of the methanol synthesis will occur at temperatures that are too low (T < 500 K, Section 5.4), and low pressures are wanted in the industry to reduce costs in methanol manufacturing. Industrial methanol plants consists of a series of adiabatic beds with cold synthesis gas injected between the beds to keep the temperature increase during methanol synthesis under control (11). The standard enthalpy of formation of the methanol process is $\Delta H = -49$ kJ mol^{-1}, equal to the value predicted by our model.

Thermodynamic functions can be derived from the canonical partition function by standard techniques (4, 45). An investigation of the change in enthalpy and Gibbs free energy for each reaction step in our model has been performed at 2 atm, 543 K, and θ = 0.5 for each species (Figs. 5 and 6). The location of the levels in Figs. 5 and 6 changes with temperature, since ΔH and ΔG are temperature dependent.

The chemisorption of the gas phase components is exothermic ($\Delta H < 0$) and endergonic ($\Delta G > 0$) as a result of the entropy decrease. The positive change in Gibbs free energy at chemisorption indicates that the steady-state equilibrium coverages of the species are small. The ordering of the steps indicates that the coverage of methoxide is low compared to the coverage of methanol, and that the coverage of $H_2COO\star$ is low compared to formate.

5.4. Coverage of Intermediates

Calculated coverages of the species are shown in Table 4. The values of the shift reaction intermediates are almost identical to previous published data (8).

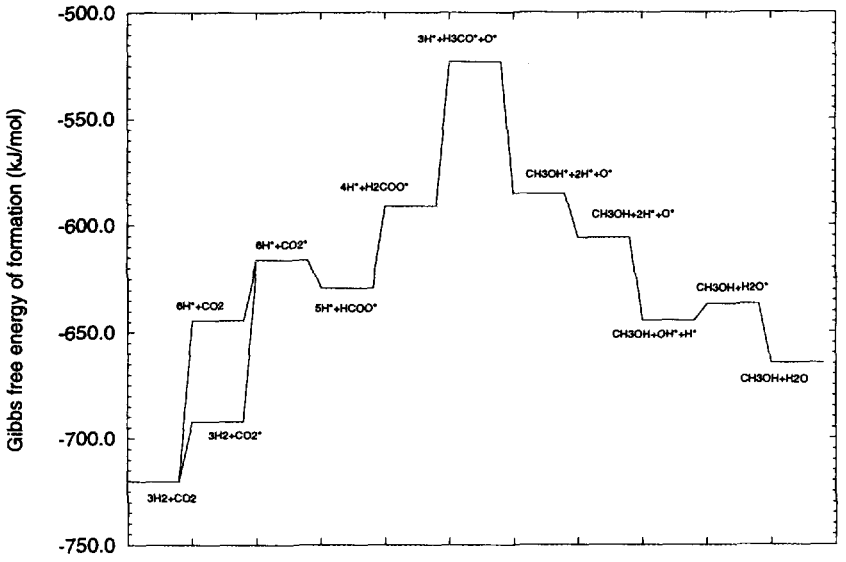

FIG. 6. Gibbs free energy of formation on Cu(111) at T = 543 K, p = 2 atm, and θ = 0.5 for the methanol synthesis.

At low pressure p = 2 bar, temperature T = 500 K, and gas composition $H_2:CO_2:CO:H_2O:CH_3OH$ = 89.49 : 4.49 : 5.49 : 0.51 : 0.02 corresponding to an 84.81% approach to equilibrium, the abundant species were free sites $\theta_* \approx 0.88$ and hydrogen $\theta_{H*} \approx 0.11$. The approach to equilibrium is defined here as the ratio of the actual reaction quotient to the equilibrium constant. At high pressure p = 50 bar, temperature T = 500 K, and at gas composition $H_2:CO_2:CO:H_2O:CH_3OH$ = 88.65 : 3.65 : 1.79 : 1.35 : 4.56 corresponding to a 87.19% approach to equilibrium, the abundant species were free sites $\theta_* \approx 0.52$, hydrogen $\theta_{H*} \approx 0.33$, and formate $\theta_{HCOO*} \approx 0.07$.

The value of θ_{O*} is very small, indicating that methanol is formed on an essentially oxygen-free Cu surface. This result is supported by the work of Muhler *et al.* (21), who measured the response in methanol activity *in situ* on a working catalyst adding CO and CO_2 as pulses and steps to the reaction gas mixture. The *in situ* probing of θ_{O*} deduced from the transient behavior of methanol formation clearly demonstrated no significant amount of oxide on the Cu surface.

The predicted relative large coverage of formate has been verified with a recent *in situ* infrared vibration spectroscopy study by Millar *et al.* (23). A significant steady-state concentration of copper formate was measured under typical industrial operating conditions. Methoxide and H_2COO* were not detected on the copper component, but this observation is not in disagreement with our work, since the model predictions of θ_{H_3CO*} and θ_{H_2COO*} are very small and therefore hardly detectable.

The coverage of the intermediates were almost constant at the industrial working conditions p = 50 bar and T = 493–573 K. Below 500 K formate became the abundant species with $\theta_{HCOO*} \approx 1$ at $T \leq 400$ K, and a complete blocking of the free sites occurred.

TABLE 4

Coverage of Species on Cu(111) at T = 500 K with a Gas Composition Corresponding to Approximately 85% Approach to Equilibrium (Section 5.4)

Coverage of species	p = 2 bar	p = 50 bar
$\theta*$	8.80×10^{-1}	5.20×10^{-1}
θ_{H*}	1.10×10^{-1}	3.30×10^{-1}
θ_{HCOO*}	1.20×10^{-3}	7.00×10^{-2}
θ_{O*}	2.40×10^{-6}	3.90×10^{-6}
θ_{H_2O*}	4.50×10^{-5}	1.70×10^{-3}
θ_{OH*}	2.20×10^{-3}	1.70×10^{-2}
θ_{CO*}	3.30×10^{-3}	1.60×10^{-2}
θ_{CO_2*}	2.30×10^{-4}	2.80×10^{-3}
θ_{CH_3OH*}	1.80×10^{-5}	4.20×10^{-2}
θ_{H_3CO*}	4.60×10^{-11}	2.20×10^{-8}
θ_{H_2COO*}	1.70×10^{-8}	4.90×10^{-6}

5.5. *Activation Enthalpy*

The overall activation enthalpy is defined by the formula

$$H^{\ddagger} = k_B T^2 \left(\frac{d \ln r_+}{dT}\right)_p, \qquad [38]$$

with a solution too large to be reproduced here.

A simplification of $H^{\ddagger}$ can be performed, if one of the

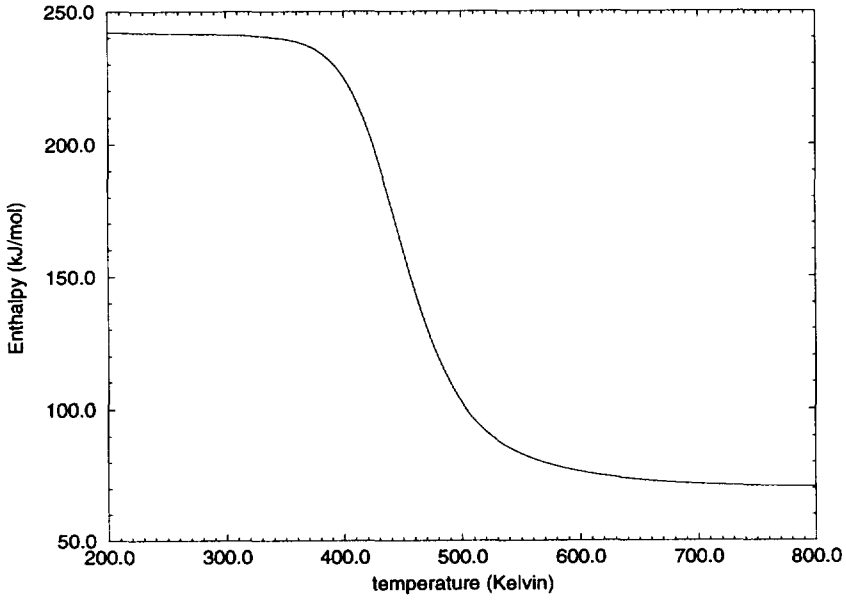

FIG. 7. Activation enthalpy versus temperature with gas composition $H_2:CO_2:CO = 90:5:5$ and pressure $p = 50$ bar on Cu(111).

slow steps in the redox mechanism makes several turnovers in both directions for each net turnover of the WGS reaction,

$$\begin{aligned} H^{\ddagger} = {} & H^{\ddagger}_{11} + H_{11} - \frac{3}{2}H_5 - H_8 + H_9 + H_{10} \\ & + H_5\theta_{H\star} - 2H_1\theta_{H_2O\star} - 2H_6\theta_{CO\star} + 2H_8\theta_{CO_2\star} \\ & + 2\left(\frac{1}{2}H_5 + H_8 - H_9\right)\theta_{HCOO\star} \\ & + 2(H_5 + H_8 - H_9 - H_{10})\theta_{H_2COO\star} \\ & + 2\left(-\frac{1}{2}H_5 + H_{12} + H_{13}\right)\theta_{H_3CO\star} + 2H_{13}\theta_{CH_3OH\star} \\ & - 2(H_1 + 2H_2 + H_3 + H_5)\theta_{O\star} \\ & - 2\left(H_1 + H_2 + \frac{1}{2}H_5\right)\theta_{OH\star}. \end{aligned} \quad [39]$$

Temperature and surface concentrations of the reaction intermediates will determine the value of $H^{\ddagger}$. The sum of the product terms is the average cost in energy to create two free sites required in the rate-limiting step

$$\frac{3}{2}H_2(g) + CO_2(g) + 2\star \rightleftharpoons H_3CO\star + O\star. \quad [40]$$

The activation enthalpy of the methanol synthesis at $p = 50$ bar and a gas composition of $H_2:CO:CO_2 = 90:5:5$ was calculated to be $H^{\ddagger} = 75$–100 kJ mol^{-1} in the temperature interval 500–580 K (Fig. 7). The dramatic increase of the overall activation enthalpy $H^{\ddagger}$ below 500 K can be explained by an increasing coverage of formate (Section 5.4). The cost in energy H_{site} to create two free sites will become significant,

$$\begin{aligned} H_{site} &\approx (H_5 + 2H_8 - 2H_9) \times \theta_{HCOO\star} \\ &\approx 175 \text{ kJ mol}^{-1} \times \theta_{HCOO\star}. \end{aligned} \quad [41]$$

The methanol process will become self-inhibiting below 500 K, due to site blocking by the stable formate species.

The pressure dependence of the overall activation enthalpy $H^{\ddagger}$ can be seen in Fig. 8. The calculated value of $H^{\ddagger}$ changes from $H^{\ddagger} \approx 66$ kJ mol^{-1} at $p = 1$ bar to $H^{\ddagger} \approx 120$ kJ mol^{-1} at $p = 100$ bar. An increase of the total pressure will reduce the coverage of free sites and the activation enthalpy will thus increase with pressure.

Typical working conditions for the industrial synthesis of methanol are $H_2:CO:CO_2 = 90:5:5$, $p = 50$–100 bar, and $T = 493$–573 K (11, 12). This temperature range ensures a low overall activation energy predicted by the model (Fig. 7).

The activation energy was calculated to be $H^{\ddagger} = 68.3$ kJ mol^{-1} at 2 bar, at 543 K, and with gas composition $H_2:CO_2 = 1:1$. This result is in agreement with the value $H^{\ddagger} = 69 \pm 4$ kJ mol^{-1} estimated from a Cu single-crystal experiment by Rasmussen *et al.* (22), and a indication of the validity of our kinetic model.

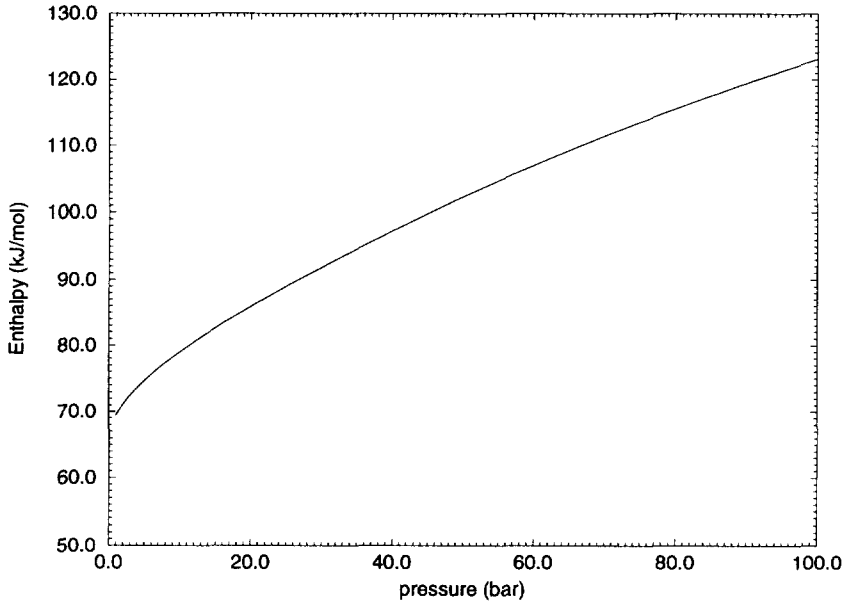

FIG. 8. Activation enthalpy versus pressure with gas composition $H_2:CO_2:CO = 90:5:5$ and $T = 500$ K on Cu(111).

5.6 Reaction Orders

The reaction orders α_i are defined by

$$\alpha_i = \left(d \ln r_+ / d \ln \frac{p_i}{p_o} \right) \qquad [42]$$

The derived expressions of α_i, which are too large to be shown here, were dependent on the surface concentrations of the reaction intermediates, and thus highly dependent on the temperature and pressure.

Reaction orders of H_2, CO_2, and CO have been calculated using a typical methanol synthesis gas mixture of $H_2:CO_2:CO = 90:5:5$ at total pressure $p = 50$ bar (Fig. 9). The variation of α_{H_2} and α_{CO_2} can be explained by the change in formate coverage upon going from $\theta_{HCOO\star} \approx 1$ at $T = 400$ K to $\theta_{HCOO\star} \approx 10^{-4}$ at $T = 800$ K. Reaction orders in the low-temperature domain with a high coverage of formate are $\alpha_{H_2} = 1/2$, $\alpha_{CO_2} = -1$, and $\alpha_{CO} = 0$. Reaction orders in the high-temperature domain with a low coverage of formate are $\alpha_{H_2} \approx 3/2$, $\alpha_{CO_2} = 1$, and $\alpha_{CO} = 0$. The coverage of free sites at $T \leq 400$ K is very small due to the blocking by the stable and abundant formate species. This self-inhibiting feature of the methanol synthesis is indicated by the negative value of $\alpha_{CO_2} = 1 - 1$. The variation of the reaction orders in the relevant temperature range of methanol synthesis $T = 493$–573 K (11, 12) are $\alpha_{H_2} = 1.0$–1.3, $\alpha_{CO_2} = 0.8$–1.0, and $\alpha_{CO} \approx 0.0$.

Pressure variations will have an impact on the reaction orders through a change in equilibrium coverages of the species. Figure 10 shows the reaction orders as a function of pressure at temperature $T = 500$ K and feed gas composition $H_2:CO_2:CO = 90:5:5$. At pressure $p = 1$ bar the reaction orders are $\alpha_{H_2} = 1.4$, $\alpha_{CO_2} = 1.0$, and $\alpha_{CO} = 0.0$. At pressure $p = 100$ bar we have $\alpha_{H_2} = 0.95$, $\alpha_{CO_2} = 0.58$, and $\alpha_{CO} = -0.14$ (Fig. 10). The decrease in reactions orders going to higher pressures indicate that the methanol process will be inhibited due to a reduction of free sites.

The calculated reaction orders with a gas composition of $H_2:CO_2 = 1:1$, a temperature $T = 543$ K, and a total pressure of $p = 2$ bar were $\alpha_{H_2} = 1.44 \approx 3/2$ and $\alpha_{CO_2} = 1.00$. The model predictions are consistent with results from a Cu single-crystal experiment (22), where the rate of methanol synthesis was observed to scale with the total pressure as $p^{2.36 \pm 0.14}$ (22).

6. CONCLUSIONS

We have formulated a kinetic model for the synthesis of methanol. The kinetic model is based on a reaction mechanism deduced from Cu single-crystal experiments. The water–gas shift reaction was implemented in the kinetic model, since this process competes with the methanol synthesis reaction on the working catalyst. No adsorbate–adsorbate interactions have been introduced in the model, except for the usual nearest neighbor repulsion limiting the saturation coverage to one molecule per site.

With data from methanol synthesis on a Cu(100) single crystal (22) the rate-limiting step in the reaction mechanism of methanol synthesis was found to be the hydrogenation of $H_2COO\star$ to methoxide and oxide (step 11 in Table 1). Measured rates of methanol synthesis (22) at pressures

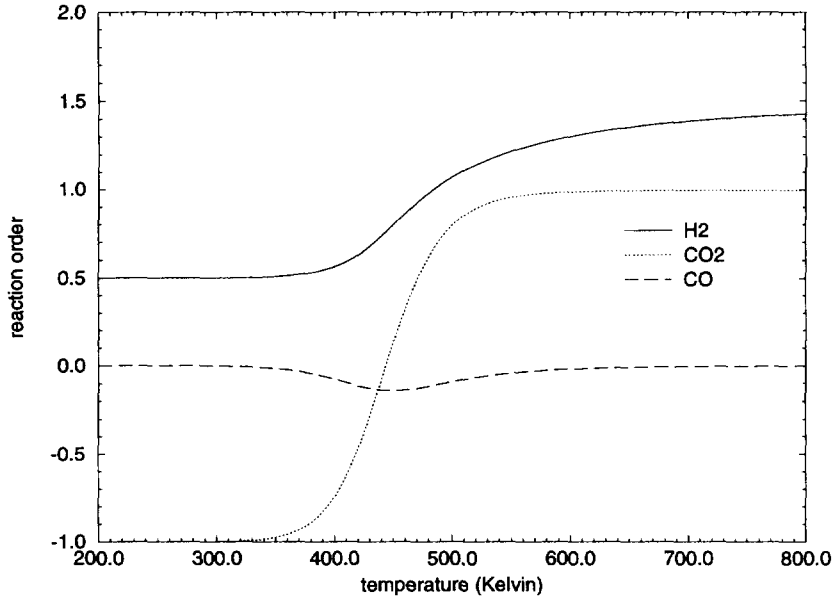

FIG. 9. Reaction order versus temperature with gas composition $H_2:CO_2:CO = 90:5:5$ and pressure $p = 50$ bar on Cu(111).

$p = 1$–4 bar, temperatures $T = 483$–563 K, and varying gas mixtures of CO_2 and H_2 were reproduced by the model.

An investigation of the coverages of the intermediates showed that hydrogen and formate were the abundant species under industrial working conditions of the methanol synthesis (493–573 K and 50–100 bar). A self-inhibition of the methanol synthesis was predicted by the model at temperatures below 500 K due to the blocking of free sites by the stable and abundant formate species.

The overall activation enthalpy of methanol synthesis was calculated to be $H^{\ddagger} = 75 - 100$ kJ mol^{-1} in the temperature interval $T = 500$–580 K with a gas composition $H_2:CO:CO_2 = 90:5:5$ and total pressure of 50 bar. A considerable increase of $H^{\ddagger}$ was predicted at temperatures below 500 K due to the blocking of free sites by the formate species. The model prediction of $H^{\ddagger} = 68.3$ kJ mol^{-1} at $T = 543$ K, $p = 2$ bar, and gas composition $H_2:CO_2 = 1:1$ is consistent with an estimated activation enthalpy

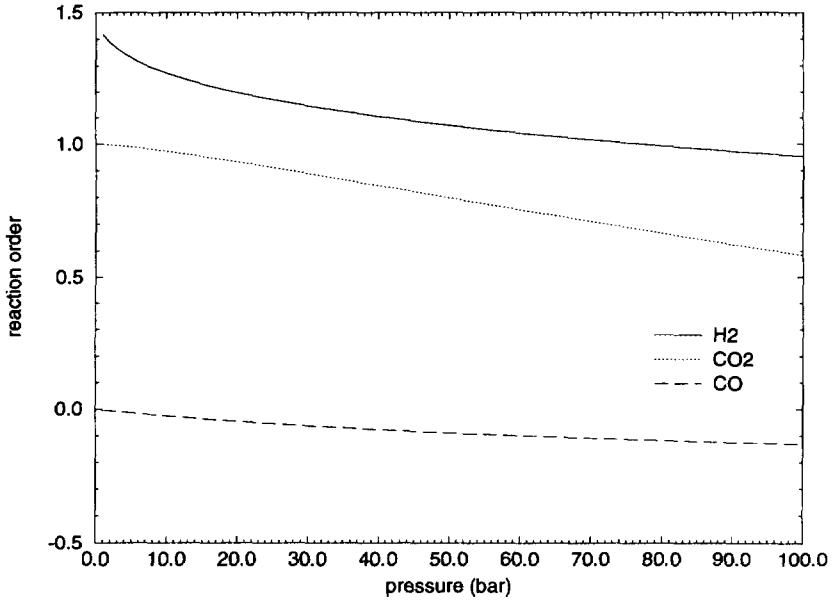

FIG. 10. Reaction orders versus pressure with gas composition $H_2:CO_2:CO = 90:5:5$ and $T = 500$ K on Cu(111).

$H^{\ddagger} = 69 \pm 4$ kJ mol^{-1} from Cu(100) single-crystal experiments (22).

The reaction orders in the temperature range $T = 493$–573 K with a gas mixture of $H_2:CO_2:CO = 90:5:5$ were calculated to be $\alpha_{H_2} = 1.0$–1.3, $\alpha_{CO_2} = 0.8$–1.0, and $\alpha_{CO} \approx 0.0$ at a constant pressure of $p = 50$ bar. The reaction orders with a gas composition of $H_2:CO_2:CO = 90:5:5$ and at constant temperature $T = 500$ K changed from $\alpha_{H_2} = 1.4$, $\alpha_{CO_2} = 1.0$, $\alpha_{CO} = 0.0$ at a low pressure of $p = 1$ bar to $\alpha_{H_2} = 0.95$, $\alpha_{CO_2} = 0.58$, $\alpha_{CO} = -0.14$ at a high pressure of $p = 100$ bar. The model predictions of $\alpha_{H_2} = 1.44 \approx 3/2$ and $\alpha_{CO_2} = 1.00$ at a temperature of $T = 543$ K, a pressure of $p = 2$ bar, and a gas composition of $H_2:CO_2 = 1:1$ are in agreement with Cu(100) single-crystal experiments of methanol synthesis (22), where the rate of methanol synthesis was observed to scale with the total pressure as $p^{2.36 \pm 0.14}$.

The kinetic model was extrapolated to industrial working conditions of real catalysts (38, 39, 41, 42). The WGS rates (38, 39) were reproduced with great success, and the calculated methanol rates were in reasonable accordance with the measured catalyst rates (41, 42). It was only possible to obtain good model predictions with Cu(111) input parameters, and our results thus indicate that copper is the catalytically active component in industrial methanol catalysts with a dominant (111)-facet.

ACKNOWLEDGMENTS

This work was supported by the Danish Research Councils through the Center for Surface Reactivity. We thank P. B. Rasmussen, I. Chorkendorff, B. S. Clausen, and E. Törnqvist for providing experimental results for this work. The Center for Atomic-Scale Materials Physics is sponsored by the Danish National Research Foundation.

REFERENCES

1. Dumesic, J. A., Rudd, D. F., Aparicio, L. M., Rekoske, J. E., and Trevino, A. A., "The Microkinetics of Heterogenous Catalysis." Am. Chem. Soc., 1993.
2. Stoltze, P., and Nørskov, J. K., *Phys. Rev. Lett.* **55,** 2502 (1985).
3. Oh, S. H., Fisher, G. B., Carpenter, J. E., and Goodman, D. W., *J. Catal.* **100,** 360 (1986).
4. P. Stoltze, *Phys. Scr.* **36,** 824 (1987).
5. Dumesic, J. A., and Trevino, J. A., *J. Catal.* **116,** 119 (1989).
6. Helsing, B., Kasemo, B., and Zhdanov, V. P., *J. Catal.* **132,** 210 (1991).
7. Fassihi, M., Zhdanov, V. P., Rinnemo, M., Keck, K.-E., and Kasemo, B., *J. Catal.* **141,** 438 (1993).
8. Ovesen, C. V., Stoltze, P., Nørskov, J. K., and Campbell, C. T., *J. Catal.* **134,** 445 (1992).
9. Torniainen, P. M., Chu, X., and Schmidt, L. D., *J. Catal.* **146,** 1 (1994).
10. Ovesen, C. V., "Kinetic Modeling of Reactions on Cu Surfaces," Ph.D. thesis, Laboratory of Applied Physics, 1992.
11. Chinchen, G. C., Denny, P. J., Jennings, J. R., Spencer, M. S., and Waugh, K. C., *Appl. Catal.* **36,** 1 (1988).
12. Dybkjær, I., *Chem. Econ. Eng. Rev.* **13,** 17 (1981).
13. Klier, K., *Adv. Catal.* **31,** 243 (1982).
14. Chinchen, G. C., Waugh, K. C., and Whan, D. A., *Appl. Catal.* **25,** 101 (1986).
15. Chinchen, G. C., Hay, C. M., Vandervell, H. D., and Waugh, K. C., *J. Catal.* **103,** 79 (1987).
16. Fleish, T. H., and Mieville, R. L., *J. Catal.* **90,** 165 (1984).
17. Clausen, B. S., Steffensen, G., Fabius, B., Villadsen, J., Feidenhaus'l, R., and Topsøe, H., *J. Catal.* **132,** 524 (1991).
18. Chinchen, G. C., Denny, P. J., Parker, D. G., Spencer, M. S., Waugh, K. C., and Whan, D. A., *Appl. Catal.* **30,** 333 (1987).
19. Kagan, Yu. B., Liberov, L. G., Slivinskii, E. V., Loktev, S. M., Lin, G. I., Rozovskii, A. Ya., and Bashkirov, A. N., *Dokl. Akad. Nauk SSSR* **221,** 1093 (1975).
20. Liu, G., Willcox, D., Garland, M., and Kung, H., *J. Catal.* **90,** 139 (1984).
21. Muhler, M., Törnqvist, E., Nielsen, L. P., Clausen, B. S., and Topsøe, H., *Catal. Lett.* **14,** 241 (1992).
22. Rasmussen, P. B., Holmblad, P. M., Askgaard, T. S., Ovesen, C. V., Stoltze, P., Nørskov, J. K., and Chorkendorff, I., *Catal. Lett.* **26,** 373 (1994).
23. Millar, G. J., Rochester, C. H., and Waugh, K. C., *Catal. Lett.* **14,** 289 (1992).
24. Nakamura, J., Campbell, J. M., and Campbell, C. T., *J. Chem. Soc. Faraday Trans.* **86,** 2725 (1990).
25. Campbell, C. T., and Daube, K. A., *J. Catal.* **104,** 109 (1987).
26. Nakamura, J., Rodriguez, J. A., and Campbell, C. T., *J. Phys. Condens. Matter.* **1,** SB149 (1989).
27. Kiennemann, A., Idriss, H., Hindermann, J. P., Lavalley, J. C., Vallet, A., Chaumette, P., and Courty, Ph., *Appl. Catal.* **59,** 165 (1990).
28. Bowker, M., Hadden, R. A., Houghton, H., Hyland, J. N. K., and Waugh, K. C., *J. Catal.* **109,** 263 (1988).
29. Taylor, P. A., Rasmussen, P. B., Ovesen, C. V., Stoltze, P., and Chorkendorff, I., *Surf. Sci.* **261,** 191 (1992).
30. Stuve, E. M., and Madix, R. J., *Surf. Sci.* **119,** 279 (1982).
31. Wachs, I., and Madix, R. J., *Appl. Surf. Sci.* **5,** 426 (1980).
32. Wachs, I., and Madix, R. J., *Surf. Sci.* **84,** 375 (1979).
33. Bowker, M., and Madix, R. J., *Surf. Sci.* **95,** 190 (1980).
34. Sexton, B. A., Hughes, A. E., and Avery, N. R., *Surf. Sci.* **155,** 366 (1985).
35. Wachs, I. E., and Madix, R. J., *J. Catal.* **53,** 208 (1978).
36. Chorkendorff, I., Taylor, P. A., and Rasmussen, P. B., *J. Vac. Sci. Technol. A* **10,** 2277 (1992).
37. Iglesia, E., and Boudart, M., *J. Catal.* **81,** 204 (1983).
38. van Herwijnen, T., and de Jong, W. A., *J. Catal.* **63,** 83 (1980).
39. van Herwijnen, T., Guczalski, R. T., and de Jong, W. A., *J. Catal.* **63,** 94 (1980).
40. Nielsen, O. H., Sethna, J. P., Stoltze, P., Jacobsen, K. W., and Nørsk., J. K., *Europhys. Lett.* **26,** 51 (1994).
41. Stamhuis, E. J., Graaf, G. H., and Beenackers, A. A. C. M., *Chem. Ing. Sci.* **43,** 3185 (1988).
42. Graaf, G. H., Ph.D. thesis, Rijksuniversiteit Groningen, 1988.
43. Askgaard, T., "Catalytic Reaction Mechanisms," Ph.D. thesis, Physics Department, Technical University of Denmark, 1994.
44. Clausen, B. S., Schiotz, J., Gråbæk, Ovesen, C. V., Jacobsen, K. W., Nørskov, J. K., and Topsøe, H., *Catal. Lett.*, in press.
45. McQuarrie, D. A., "Statistical Mechanics." Harper & Row, New York, 1976.